Multi-parameter FWI of broadband data: beyond high resolution images

Ludovic Métivier, Romain Brossier, Serge Sambolian, Alizia Tarayoun

Multi-parameter FWI of broadband data: beyond high resolution images

L. Métivier[1,2], R. Brossier[2], S. Sambolian[3], A. Tarayoun[2]

[1]CNRS, Univ. Grenoble Alpes, LJK, F-38058 Grenoble, France
[2]Univ. Grenoble Alpes, ISTerre, F-38058 Grenoble, France
[3]Université de Strasbourg, CNRS, Institut Terre et Environnement de Strasbourg, UMR 7063, F-67084 Strasbourg, France

January 12, 2024

Main objectives

This abstract presents a multi-parameter FWI of broadband OBC data from the North Sea up to 22.5 Hz. The focus of the study is the ability of such inversion to efficiently constrain secondary parameters such as density and quality factor, beyond the building of high resolution reflectivity images derived from the impedance.

New aspects covered

1. The inversion is performed in the 3D VTI visco-acoustic approximation. A fully scalable modeling and inversion code is set up, exploiting three nested parallelization levels (MPI+MPI+OpenMP). The application is ran on more than 50 000 cores on a recently set up national HPC center in CINES, France.

2. Reflectivity images derived from the impedance are compared at 10 Hz and 22.5 Hz to highlight the gain in resolution.

3. The quality of the reconstructed density is assessed through the comparison with a density log which shows a good agreement especially in the central part between 1.5 km and 2 km depth.

4. The quality of the reconstructed quality factor is assessed through a modeling experiment where we compare the residuals for a common-receiver-gather along a line crossing the central low-velocity anomaly. The residuals are computed with the reconstructed quality factor and with a constant quality factor. The decrease of the residuals with the reconstructed quality factor is significant for the recorded long offset wave packets traveling through the low velocity anomaly.

Summary

While applying FWI to broadband data has recently become feasible thanks to increasing computational resources and progresses in the FWI workflow, such applications tend to focus on the reconstruction of high resolution reflectivity images derived from the acoustic impedance. This makes it possible to bypass the migration stage, simplifying nicely the inversion workflow in a single stage of FWI, and thus reducing the processing time from acquisition to interpretation. However, we think that the potential

of broadband FWI goes, beyond building high resolution reflectivity images, towards a quantitative characterization of the subsurface mechanical parameters. In this work, we try to assess on a 3D OBC data from the North Sea how increasing the frequency content of the inverted data helps to control the reconstruction of the density and the quality factor, on top of the velocity. The results we obtain are promising: the reconstructed density fit nicely an available density log down to 2 km depth, while the quality factor is shown to help fit waves which are attenuated when crossing the low-velocity zone at the center of the model.

Multi-parameter FWI of broadband data: beyond high resolution images

Recent advances in high performance computing and data processing workflow make possible the application of Full Waveform Inversion (FWI) to higher and higher frequency data, reaching the frequency band conventionally used for image building through migration. High resolution reflectivity images are computed by taking the spatial derivatives of the inverted velocity models, thus bypassing the migration stage, and reducing the processing time from acquisition to interpretation.

This is a nice simplification of the conventional imaging workflow. However, we think that the potentialities of FWI when applied to broadband data goes beyond the ability to derive directly high resolution images. FWI is indeed suppose to provide "quantitative estimates of the subsurface mechanical parameters" (Tarantola, 2005). In practice, when applied to narrow-band data, FWI reveals mainly amenable to provide higher resolution velocity models, remaining relatively insensitive to secondary parameters such as density or quality factor. However, applying FWI to broadband data should reveal its full potentialities, making it possible to compute quantitative estimates in a more stable way.

This is the question we try to address in this work by working on a 3D field data of the North sea up to 22.5 Hz, while previous applications considered 10 Hz maximum frequency. In the visco-acoustic VTI approximation, we simultaneously invert for the P-wave velocity V_P, the density ρ, and the quality factor Q_P. This is made possible by developing a fully scalable strategy relying on a triple level of parallelism over sources, domains, and OpenMP acceleration, for each step of the computation: wavefield modeling, gradient smoothing, optimization. The results we obtain show that the gain in resolution is substantial, but also that the density and the quality factor we reconstruct are correctly constrained. In particular, the reconstructed density fits fairly well an available density log in the target zone.

Method and HPC implementation

In this study we rely on the academic code TOYxDAC_TIME we develop in the frame of the SEISCOPE project (Yang et al., 2018). From a mathematical standpoint we solve the least-squares minimization problem

$$\min_m \frac{1}{2} \sum_{s=1}^{N_s} \|d_{\text{cal,s}}[m] - d_{\text{obs,s}}\|^2, \text{ st. } d_{cal,s}[m] = Ru_s[m], \; A(m)u_s = b_s, \tag{1}$$

where m gathers the subsurface mechanical parameters, N_s is the number of shots, $d_{obs,s}$ (resp. $d_{cal,s}$) is the observed (resp. calculated) data for shot s. The sth calculated data is extracted from the wavefield $u_s[m]$ by the restriction operator R. The wavefield $u_s[m]$ is the solution of a wave equation denoted by the general operator $A(m)$ for the shot position s. We consider here the 3D VTI visco-acoustic approximation, and m gathers the P-wave velocity V_P, the density ρ and the quality factor Q_P. Starting from an initial guess m^0, the FWI problem is solved using the following recurrence

$$m^{k+1} = m^k + \alpha^k \Delta m^k, \; \Delta m^k = -Q^k \mathscr{F}^k \left(\nabla f(m^k) \right) \tag{2}$$

where α^k is a linesearch parameter satisfying the Wolfe conditions and Δm^k is the descent direction. The latter is computed from the gradient of the misfit function $\nabla f(m^k)$ after a filtering operator $\mathscr{F}^k$ is applied to it (regularization strategy) and from a l-BFGS approximation Q_k of the inverse Hessian operator $\left(\nabla^2 f(m^k)\right)^{-1}$. The filter we employ is structure-preserving: it enhances coherent structures in the gradient. It is based on a linearized anisotropic diffusion filter strategy described in Métivier et al. (2024). The gradient itself is computed thanks to the adjoint state strategy, as the sum over shots of the time-correlation between incident and adjoint fields (Plessix, 2006).

To optimize the use of parallel computational resources, we distribute the computation shot-wise using a first MPI level. The computations required for each shot are further parallelized thanks to a domain-decomposition algorithm relying on a second MPI level. A third parallelization level is then implemented for each domain using OpenMP directives. This three-level parallelization is exploited at each step: incident and adjoint wavefield computations, gradient building by time correlation, linear algebra operations required by local optimization in equation 2, diffusion-based filtering operations. This strategy makes it possible to use efficiently up to 50,000 cores in parallel as it is illustrated in the next Section.

Broadband data FWI results

The field data we consider have been acquired using Ocean Bottom Cable devices in a shallow water environment of the North Sea. Over 50,000 shot positions are available for 2048 receivers deployed along cables, covering a surface of approximately 145 km^2. The main target is a low velocity anomaly and the structures below it, which are difficult to reconstruct, the low velocity anomaly acting as a screen for these underlying structures.

We separate the data in 8 bands of increasing bandwidth from 3 - 5 Hz to 3 - 22.5 Hz to use a conventional multi-scale workflow, from a 70 m Cartesian mesh ($\simeq 6 \times 10^6$ unknowns) to a 17.5 m Cartesian mesh ($\simeq 3.6 \times 10^8$ unknowns). We use the reciprocity to reduce the number of shots to 2048 instead of 50,000. For each band, we use a shot subsampling strategy: 16 groups of 128 randomly selected shots are constituted, and 3 l-BFGS iterations are performed on each group for a total of 48 iterations per band. On the finest grid, we use 192 domains for each shot, with 2 OpenMP for each domain, for a total of 384 cores per shot, and 49 152 cores for the whole FWI process. The elapsed time for one FWI on the finest grid is approximately 20 hours, for a total of almost 1 million scalar hours. This is significant for an academic project. It was made possible only because we had a special access to the ADASTRA national machine (CINES, France, HPE-Cray machine with 2×96 cores AMD-Genoa nodes at 2.4 GHz) during summer 2023 before it went on production for the whole French academic community.

We present in Figure 1 the configuration of the OBC acquisition superimposed with a constant depth slice ($z = 1000$ m) of the velocity model reconstructed at 22.5 Hz. We see how the low velocity is finely reconstructed, with a visible network of connected faults. The blue dots represent the receiver position along the cables, while the small grey dots represent the position of the 50,000 shots.

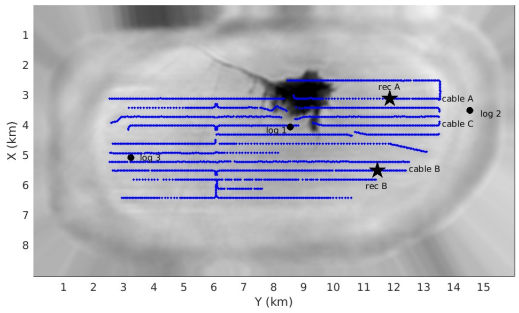

Figure 1 Acquisition layout superimposed to a constant depth slice at $z = 1000$ m of the final velocity model inverted up to 22.5 Hz. The blue dots denote the cables geometry. Log 1 indicates the position of the well where the velocity and density logs have been measured in Figures 3 and 4 respectively. Rec A indicates the position of the receiver for the CRG displayed in Figure 6 for a line of sources along cable A, crossing the low-velocity anomaly.

In Figure 2, we compare two reflectivity images $r(\mathbf{x})$ at 10 Hz and 22.5 Hz extracted along Cable C, in the periphery of the low velocity anomaly (see Fig 1). They are built as the vertical derivative of the acoustic impedance: $r(\mathbf{x}) = \partial_z (v_P(\mathbf{x})\rho(\mathbf{x}))$. The resolution gain at 22.5 Hz is striking, especially in the shallow part above 1.5 km depth. The deep reflector at 3.5 km depth appears also much more clearly.

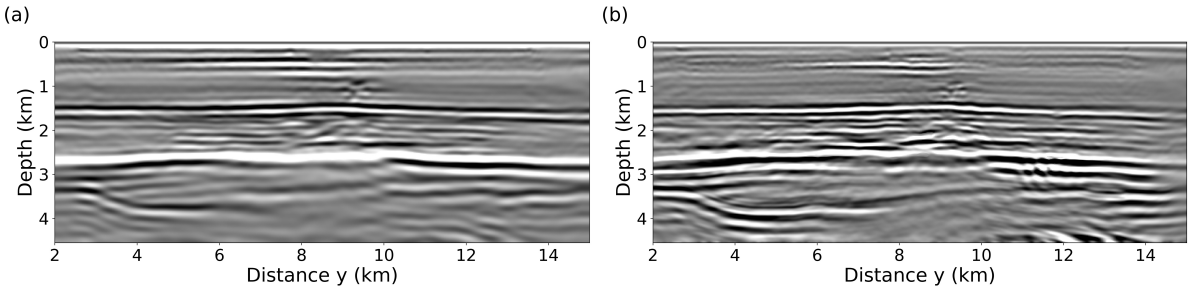

Figure 2 *Reflectivity images derived from P-wave velocity and density at (a) 10 Hz, (b) 22.5 Hz.*

In Figures 3 and 4, we present the same vertical slice along Cable C for the velocity and the density models reconstructed at 22.5 Hz. We superimpose the log values and the corresponding vertical profiles at the position of log 1. We present on the right of the two Figures the well log comparison alone, where we add the profile at 10 Hz. We can observe that between 10 Hz and 22.5 Hz, the fit to the sonic and density log improves significantly, notably between 1.5 km and 2 km depth. We can see how well the

density fits the log in this zone.

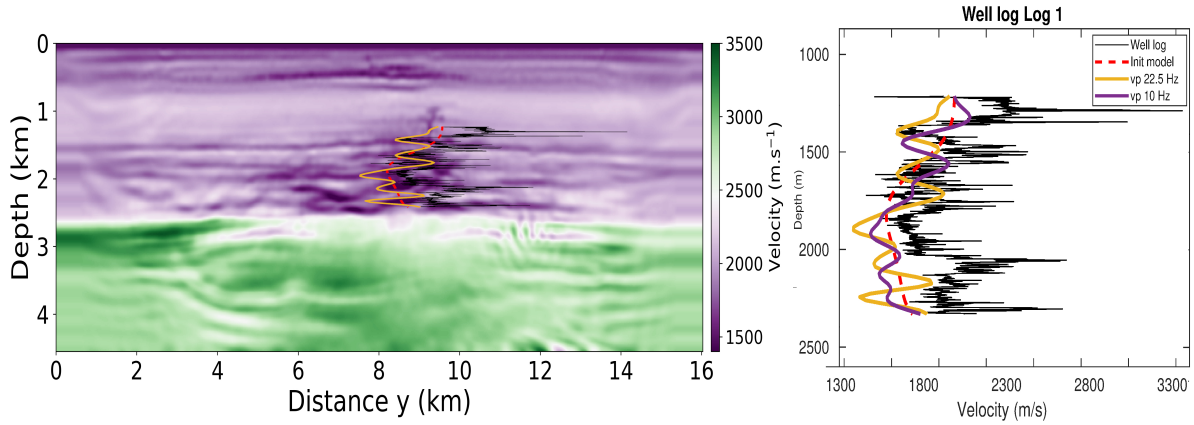

Figure 3 *Left: Slice of the velocity model at 22.5 Hz along Cable C, with sonic log 1 superimposed. Right: sonic log comparison with the initial velocity model, velocity model at 10 Hz, velocity model at 22.5 Hz.*

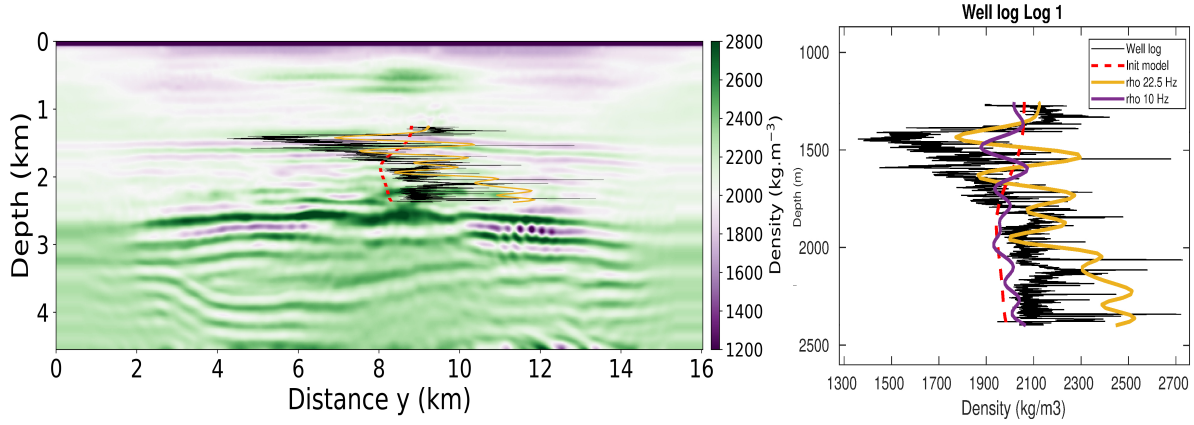

Figure 4 *Left: Slice of the density model at 22.5 Hz along Cable C, with sonic log 1 superimposed. Right: density log comparison with the initial density model, density model at 10 Hz, density model at 22.5 Hz.*

In Figure 5 we present a 3D view of the central zone of the reconstructed model for both V_P and Q_P. We can see again how well detailed is the central low velocity anomaly, but also that the Q_P model is consistent with the structure of the low velocity anomaly: Q_P decreases down to values as low as 57 in zones of slow velocity. To control the meaningfulness of the Q_P model we perform modeling in the final reconstructed model at 22.5 Hz and compute the residuals for a common-receiver-gather aligned with Cable A, crossing the low velocity zone. We repeat the same experiment with a constant Q_P model, with a value fixed at 200 except in the water layer where it is fixed at 1000. We compare the residuals in Figure 6. We can observe a significant decrease of the residuals with the reconstructed Q_P for the long offset diving part of the data. These waves go through the central part of the model and are thus affected by the attenuation in this zone. The reconstructed Q_P model helps to fit these waves.

Conclusions

We present here an application of 3D VTI-acoustic FWI to broadband OBC data from the North Sea. Thanks to the development of a modeling and inversion code relying on three nested parallelization levels (MPI + MPI + OpenMP), we are able to invert the data up to 22.5 Hz for more than three hundred millions unknowns using simultaneously up to 50,000 cores on the French national machine ADASTRA. Our results indicate that beyond high resolution, inverting broadband data using FWI should bring

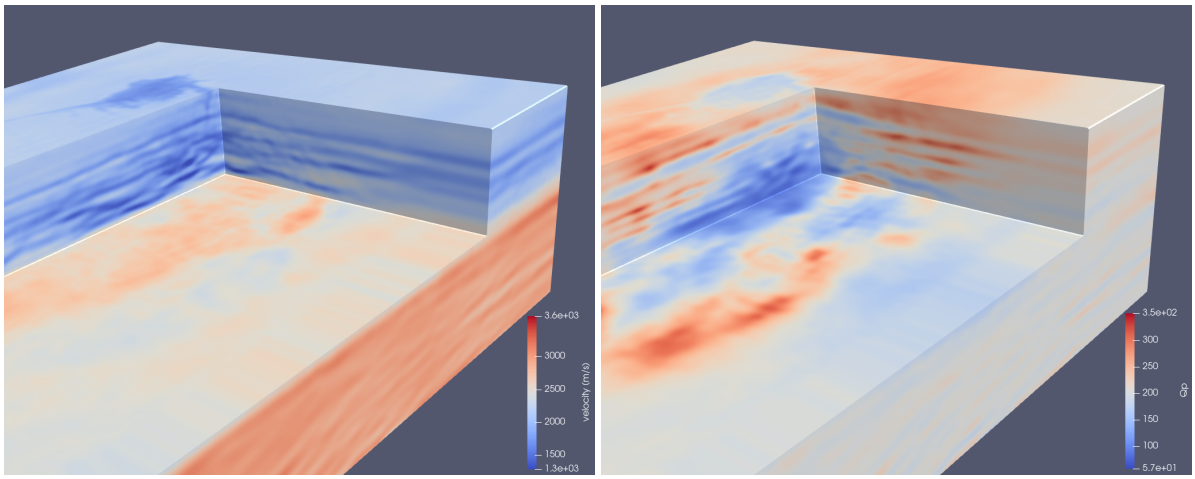

Figure 5 *3D view of the central target for (a) the velocity model at 22.5 Hz, (b) the quality factor Q_P at 22.5 Hz.*

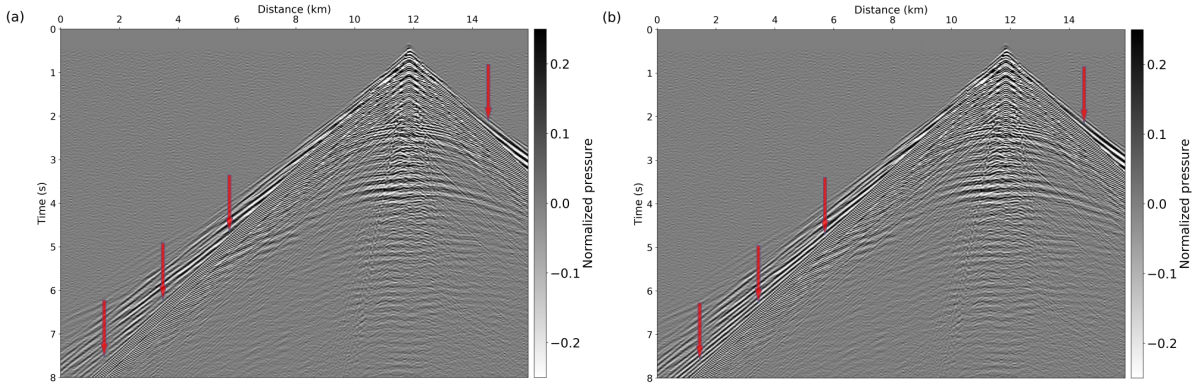

Figure 6 *Common receiver gathers residuals at 22.5 Hz for computed with (a) the final estimated Q_p model (b) a constant $Q_p = 200$ model.*

quantitative estimates of the velocity and secondary parameters such as density and quality factor.

Acknowledgments

This study was partially funded by the SEISCOPE consortium (`http://seiscope2.osug.fr`), sponsored by AKERBP, CGG, DUG, EXXONMOBIL, GEOLINKS, JGI, PETROBRAS, SHELL, SINOPEC and TOTALENERGIES. This study was granted access to the HPC resources provided by the GRICAD infrastructure (https://gricad.univ-grenoble-alpes.fr), Cray Marketing Partner Network (`https://partners.cray.com`) and IDRIS/TGCC/CINES under the allocation 046091 made by GENCI.

References

Métivier, L., Brossier, R., Hoffmann, A., Mirebeau, J.M., Provenzano, G., Tarayoun, A. and Yong, P. [2024] Coherence-enhancing anisotropic diffusion filter for 3D high resolution reconstruction of P-wave velocity and density using full waveform inversion: application to a North Sea Ocean Bottom Cable dataset. *Geophysics*, **89**(1), R33–R58.

Plessix, R.E. [2006] A review of the adjoint-state method for computing the gradient of a functional with geophysical applications. *Geophysical Journal International*, **167**(2), 495–503.

Tarantola, A. [2005] *Inverse Problem Theory and Methods for Model Parameter Estimation*. Society for Industrial and Applied Mathematics, Philadelphia.

Yang, P., Brossier, R., Métivier, L., Virieux, J. and Zhou, W. [2018] A Time-Domain Preconditioned Truncated Newton Approach to Multiparameter Visco-acoustic Full Waveform Inversion. *SIAM Journal on Scientific Computing*, **40**(4), B1101–B1130.